A double-panel active segmented partition module using decoupled analog feedback controllers: Numerical model

Jason D. Sagers
Department of Mechanical Engineering, Brigham Young University, Provo, Utah 84602

Timothy W. Leishman
Department of Physics and Astronomy, Brigham Young University, Provo, Utah 84602

Jonathan D. Blotter
Department of Mechanical Engineering, Brigham Young University, Provo, Utah 84602

(Received 17 July 2008; revised 11 March 2009; accepted 20 March 2009)

Low-frequency sound transmission has long plagued the sound isolation performance of lightweight partitions. Over the past 2 decades, researchers have investigated actively controlled structures to prevent sound transmission from a source space into a receiving space. An approach using active segmented partitions (ASPs) seeks to improve low-frequency sound isolation capabilities. An ASP is a partition which has been mechanically and acoustically segmented into a number of small individually controlled modules. This paper provides a theoretical and numerical development of a single ASP module configuration, wherein each panel of the double-panel structure is independently actuated and controlled by an analog feedback controller. A numerical model is developed to estimate frequency response functions for the purpose of controller design, to understand the effects of acoustic coupling between the panels, to predict the transmission loss of the module in both passive and active states, and to demonstrate that the proposed ASP module will produce bidirectional sound isolation. © *2009 Acoustical Society of America.* [DOI: 10.1121/1.3117682]

PACS number(s): 43.55.Rg, 43.50.Ki, 43.40.Vn [LMW] Pages: 3806–3818

I. INTRODUCTION

There has long been interest in the use of partitions to reduce sound transmission into noise-sensitive environments. A particular need for improvement exists at lower frequencies, where their passive sound isolation is inadequate. This is the case in both single- and double-leaf partitions wherein the transmission loss (TL) is severely degraded at lower frequencies due to resonance effects.[1] A common passive method to reduce sound transmission is to add mass to the partition. The normal-incidence mass law indicates that a 6 dB increase in the TL is possible for every doubling of the mass of the partition.[2,3] However, this solution is not feasible for many situations wherein extra weight cannot be tolerated, such as in aerospace vehicles, large ceiling structures of buildings, walls and ceilings of high-rise buildings, etc. A promising solution to the problem involves the use of active control of lightweight partitions.

Two active control strategies that have been utilized to improve the sound isolation performance of partitions at low frequencies include active structural acoustic control[4] (ASAC) and active segmented partitions (ASPs).[5] The ASAC approach typically involves actuating a continuous panel in such a way as to reduce the efficiency of acoustic radiation into the receiving space. This approach has been explored thoroughly.[4,6–15] It is typically implemented by locating several actuators over the continuous panel and by locating the sensors either on the panel or in the receiving space. A control algorithm is then used which either alters the radiating mode shapes of the panel (i.e., to make the panel a less efficient acoustic radiator) or reduces the vibration amplitudes of the existing mode shapes. The performance of the control scheme is typically quantified by using microphones to measure the attenuation in sound pressure level at several locations in the receiving space. In general, receiving-side attenuations produced by ASAC have been small, with typical results ranging from 5 to 10 dB in narrow frequency bands. However, a concise summary of ASAC performance results is difficult because the measurement techniques reported in the literature are inconsistent. The major challenges of the ASAC approach include large numbers of fully-coupled controllers, the frequent (but not exclusive) use of microphones as error sensors in the receiving space, the spatial control spillover that inevitably results when using a continuous transmitting panel, and the minimal attenuation achieved in narrow frequency bands.

The alternative classification of ASPs includes active control approaches wherein a partition is subdivided into an array of small modules that are both acoustically and mechanically segmented. The segmentation has several potential advantages. First, it allows independent control of each module, thus eliminating the impracticality of a large number of fully-coupled controllers. Second, it simplifies the active control problem by allowing the long-wavelength limit to be used with exposed module surfaces and within module cavities. If the acoustic wavelength is much larger than the module spatial dimensions, the acoustic field variables become relatively uniform over its extent. Simpler actuation, sensing, and control schemes result that may be used to increase sound isolation. Finally, the approach facilitates the placement of error sensors inside the partition (as has been occasionally tried in continuous double-leaf partitions), thus eliminating the common need for microphones in the acoustic space outside of the partition.

An effective double-panel ASP has been implemented by Leishman and Tichy.[5,16–19] Several designs for individual ASP modules were published in 2005; analytical models were used to explore two single-panel designs and two double-panel designs.[5] Experimental embodiments followed.[18,19] The single-panel analytical models included an actuator, a transmitting diaphragm, and surrounding interstitial supports between adjacent modules. One of the models assumed that the transmitting diaphragm vibrated snugly but without friction within a surrounding interstitial structure with finite impedance and considerable exposed width in the plane of the partition. The other included a resilient surround between the diaphragm and a surrounding interstitial structure that was assumed to be rigid and very thin in the plane of the partition. In both cases, the transmitting diaphragm was forced directly by the actuator. The investigations found that both designs would produce modest actively controlled TL at some frequencies but they were unable to provide much TL near the resonances of either the wide interstitial structure or the surround.

The double-panel designs used an active composite panel on the source side of the module and a passive panel on the transmitting side of the module. The active composite panel consisted of a circular control loudspeaker mounted in a larger, square, aluminum honeycomb sandwich panel. The loudspeaker acoustically actuated the module to minimize the vibration of the transmitting panel. It was found that this was accomplished through a significant reduction in the volume velocity into the cavity. An individual double-panel ASP module and a digital feed-forward controller produced experimental TL results near 80 dB over a band of 40 Hz–1.0 kHz.[18] Two different error-sensing schemes were investigated: an acoustic microphone located in the cavity and an accelerometer mounted to the transmitting panel. Similar TL results were obtained in both cases.

Although the double-panel module and controller produced very high TL, it also had several limitations, as noted by the authors. First, the digital feed-forward controller required a time-advanced reference signal. Second, it could only attenuate narrowband disturbances (i.e., it lacked broadband random noise control capabilities). Third, it had a slow convergence rate and a difficult time tracking swept-sine disturbances. Finally, the module was unidirectional and could not produce TL in both directions. Despite these limitations, the double-panel module represented a unique lightweight active partition element that exhibited such high TL capabilities over a broad bandwidth, including very low frequencies. The authors concluded that additional work would be required to assess the normal-incidence TL characteristics of other individual module configurations and multiple modules mounted in ASP arrays.

The authors began the process of addressing the second half of this recommendation by constructing two ASP arrays with four double-panel modules, each with its own digital feed-forward controller.[19] The array was tested using both centralized and decentralized controls. Centralized control was implemented by using four multiple-input/multiple-output (MIMO) controllers while decentralized control was implemented by using four single-input/single-output (SISO) controllers. The experimental ASP array under SISO control produced TL results near 55 dB over a band of 40–300 Hz. This approached the maximum measurable TL of the experimental measurement system. Surprisingly, the SISO controllers produced an average TL that was about 6 dB higher than the MIMO controllers. The result emphasized the fact that the acoustic segmentation within the double-panel ASP allowed decoupled controllers to function with an array of modules. The same limitations manifested by the individual ASP modules were evident in the array.

By way of suggestion, a practical active partition (be it an ASAC or ASP partition) should satisfy a few important criteria. First, it should be bidirectional for many applications, being capable of providing sound isolation in both directions through the partition. Second, it should be capable of controlling both tonal and broadband random disturbances. Third, it should be self-contained, meaning that all necessary sensing and actuation hardware should be located on or within the partition. Finally, the partition should provide global attenuation of acoustic energy in the receiving space.

The purpose of this paper is to introduce a new ASP module and control scheme with pertinent analytical and numerical modeling. The model will include key components of the system, including panels, sensors, actuators, and controllers. It will be used to (1) estimate the plant frequency response functions (FRFs), (2) understand the effects of acoustic coupling between the panels, (3) predict the TL of the module in both passive and active states, and (4) demonstrate that the module design will produce bidirectional sound isolation. This paper will thus demonstrate the potential of the module and its satisfaction of the design criteria. Sections II–V address the module design, its analogous circuit representation, the development of its governing equations, and various modeling predictions.

II. DESIGN CONSIDERATIONS OF THE NEW MODULE

The new ASP module incorporated choices in both the design of the physical configuration and the active control method. These two aspects are described in Secs. II A and II B.

A. Physical description

The proposed design for the module includes a stiff, lightweight panel on its source side and one on its transmitting side, separated by an air volume, as shown in Fig. 1. Each panel is connected around its perimeter to a thin, lightweight structure through a resilient connection or surround. The enclosing structure, which acts as an interstice between adjacent modules in an ASP array, is considered to be a motionless rigid body in this investigation. However, if the structure were to vibrate to some degree, as it would in a constructed partition array, it would radiate inefficiently and the resilient surrounds would allow the panels to vibrate or be controlled with substantial independence. Mechanical coupling would be reduced between the two panels in a given module and between panels of any two modules in the array, thus enhancing the possibility of successful decoupled

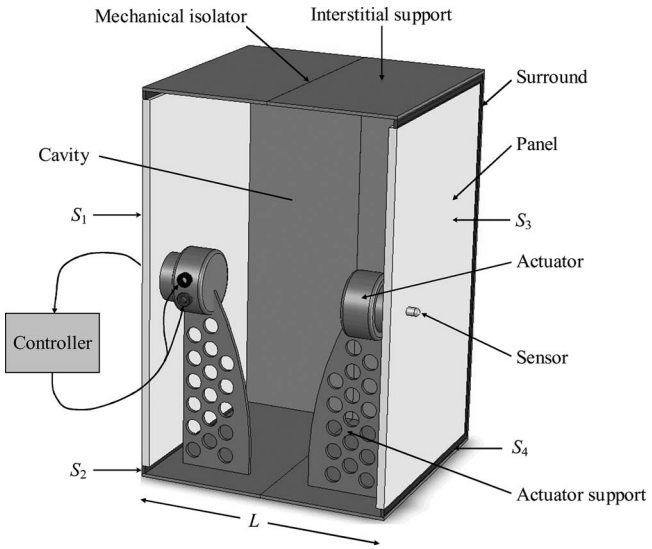

FIG. 1. Cutaway view of the double-panel ASP module.

controllers. As a further means of reducing mechanical coupling between panels in a module, and from one side of an array to the other, a resilient airtight mechanical isolator is also included between the two halves of the interstice.

An actuator and sensor pair is connected to each panel in the module. The actuators are contained inside the cavity, and the sensors can be mounted on either side of their respective panels. The actuators may be configured as inertial devices or connected to the interstitial structure by means of lightweight supports if the effects of reactive motor forces on the supports and structure are deemed insignificant. Other actuation schemes, including the use of inertial actuators, are also possible. The output of each sensor is fed into its respective controller as an error signal. The output of the controller is fed into the corresponding actuator (shown schematically for the leftmost panel in Fig. 1). Although not shown in the figure, the necessary electronics for the controllers could be compactly designed so that they are contained within the module. The remainder of the cavity is filled with fibrous acoustically absorbent material (not shown in the figure) to help improve the passive sound isolation performance of the module at higher frequencies (above the active control bandwidth).

Different types of actuators such as piezoelectric devices, inertial shakers, or moving-coil drivers could be used in the module. The actuators modeled in this paper are moving-coil drivers with magnets attached rigidly to the interstitial structure enclosing the module. Different types of sensors could likewise be used in the module. Ideal accelerometers are assumed in this paper. Although the types of actuators and sensors could be changed in a different design, it is critical to the validity of the model that all of the important dynamics of the panels, surrounds, actuators, and sensors are included.

B. Active control description

An analog feedback controller was selected for this module because of its potential for broadband control as well as its relative ease of implementation, low cost, and low

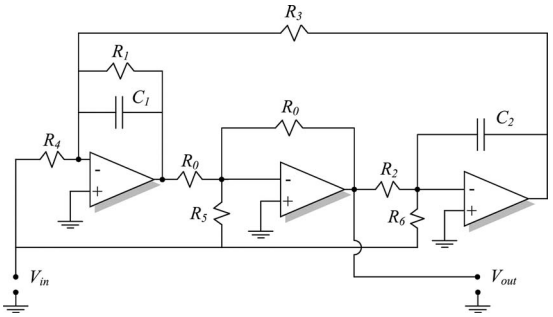

FIG. 2. Electrical schematic of a second-order Fleischer–Tow biquad circuit.

mass. Two independent controllers whose complex FRFs are represented by H_1 and H_2 were used (one for each panel). For this work, the controllers were second-order, analog Fleischer–Tow biquad circuits,[20–22] which use resistors, capacitors, and operational amplifiers to create desired transfer functions between their input and output voltages. The shape of a transfer function is determined by choosing the values of the resistors and capacitors. The electrical schematic of the controller is shown in Fig. 2.

The output voltage signal from the accelerometer becomes the input voltage to the controller (V_{in}). The output voltage from the controller (V_{out}) becomes the input voltage to the actuator. The Laplace domain transfer function between the input and output voltages of the controller is then given by the expression

$$\frac{V_{\text{out}}}{V_{\text{in}}} = -\frac{\frac{R_0}{R_5}s^2 + \frac{1}{R_1C_1}\left(\frac{R_0}{R_5} - \frac{R_1}{R_4}\right)s + \frac{1}{R_3R_6C_1C_2}}{s^2 + \frac{1}{R_1C_1}s + \frac{1}{R_2R_3C_1C_2}}. \quad (1)$$

Two important physical design choices made it possible to use a controller that was only second-order. First, it was important that collocated sensor and actuator pairs were used to eliminate undesirable delay in the plant due to acoustic propagation. Second, the airspace between the two panels was filled with absorptive material to dampen high-frequency cavity resonances which could unnecessarily complicate the control scheme.[23]

III. ANALOGOUS CIRCUIT REPRESENTATION

An analogous circuit model provides a multiple-domain (electrical, mechanical, and acoustical) representation of a system and yields a straightforward way to write its governing equations. Analogous circuit modeling techniques are used in this paper to develop the numerical model for the new ASP module. A discussion of these techniques can be found in the literature[24,25] and will not be repeated here, except as necessary to highlight specific areas of interest.

A. Physical schematic

A schematic drawing of the module is shown in Fig. 3. Each half of the module incorporates a two degree of freedom (DOF) mechanical system that resembles a moving-coil loudspeaker driver. The first DOF is contained in the motion of the panel (diaphragm), while the second DOF is contained

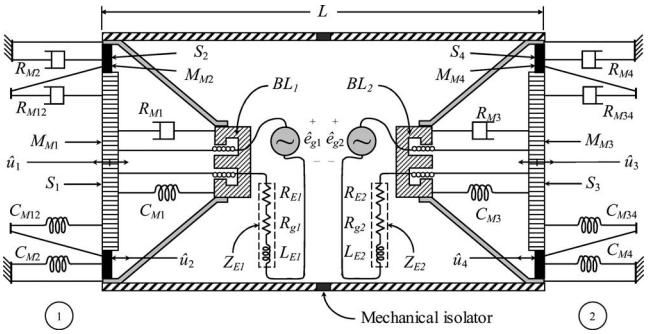

FIG. 3. Schematic view of the ASP module.

in the motion of the surround. Since the "classical" model of a loudspeaker[24,26] characterizes only a single DOF for the radiating surface, the loudspeaker model used in this paper is referred to as an "enhanced" model.

Because the two halves of the module contain identical components, only a detailed discussion of the left half will be given here. The mass of the panel is represented by M_{M1} and the mass of the surround is represented by M_{M2}. The panel and the surround each act as radiating surface areas S_1 and S_2, respectively. They are assumed to vibrate with uniform complex velocity amplitudes $\hat{u}_1$ and $\hat{u}_2$. This assumption is only valid at low frequencies as higher-order modal patterns will begin to appear in both the panel and surround at higher frequencies.

The connection between the surround and the interstitial support is modeled with a resistance and a compliance (R_{M2} and C_{M2}, respectively) as is the connection between the surround and the panel (R_{M12} and C_{M12}, respectively). These lumped elements are assumed to be distributed uniformly around the perimeter of the module face. Because of the possible asymmetry in surround properties at its inner and outer edges, R_{M2} and R_{M12} are generally not assumed to be equal, nor are C_{M2} and C_{M12}. Finally, the secondary suspension or spider of the moving-coil driver is modeled with its own resistance and compliance values R_{M1} and C_{M1}, respectively.

The moving-coil driver has intrinsic electrical properties which also describe its behavior. They have been converted to the mechanical mobility domain as an ideal flow source, with a value of $(\hat{e}_{g1}BL_1)/Z_{E1}$, in parallel with its internal mobility $Z_{E1}/(BL_1)^2$. The complex control voltage supplied by the controller as the input to the actuator is represented by $\hat{e}_{g1}$.

The benefit of using the enhanced model shown in Fig. 3 is that it allows the surround to vibrate as a lumped element, with its own DOF. As a result, it can better predict the TL that will occur if the panel vibration is reduced by the active control scheme while the surround is still permitted to vibrate. It is anticipated that any residual vibration of the surround can significantly degrade the TL performance of the module.

One of the difficulties with the enhanced model is that it requires the determination of the additional mechanical mass, resistance, and compliance values of the surround. Measurement methods exist to determine the composite parameters of the classical model,[27–38] but the individual values shown in Fig. 3 are more difficult to ascertain. To solve this problem, the authors developed a laser-based measurement method from which the unknown parameters (M_{M1}, M_{M2}, C_{M1}, C_{M2}, C_{M12}, R_{M1}, R_{M2}, R_{M12} and M_{M3}, M_{M4}, C_{M3}, C_{M4}, C_{M34}, R_{M3}, R_{M4}, R_{M34}) could be extracted. Details of the method are given elsewhere in the literature.[39]

As mentioned previously, the airspace between the two panels of the module was to be filled with a porous material to provide acoustic absorption. The attenuation coefficient α of such a material may be readily determined using a plane-wave tube,[40–42] and the resulting values may be used in the complex wave number $\tilde{k}$ of the model.

B. Analogous circuit schematic

The multiple-domain analogous circuit representation of the ASP module is shown in Fig. 4. The left and right halves of the module are represented in the left and right sides of the circuit, respectively. Eight gyrator elements were used in the circuit to couple the acoustic impedance domain and the mechanical mobility domain at various locations. The electrical components of the moving-coil driver have already been transferred from the electrical impedance domain to the mechanical mobility domain. A one-dimensional waveguide network is used in the center of the circuit to acoustically couple the left and right halves of the module and account for axial wave effects. Appropriate mechanical and acoustical grounds are represented by G_M and G_A, respectively.

Constant incident acoustic pressure sources are modeled on each side of the module with complex amplitudes $\hat{p}_{i1}$ and $\hat{p}_{i2}$. Disturbance pressures are allowed to impinge upon the device from the left (side 1), right (side 2), or both sides simultaneously. It should be noted that the analogous circuit

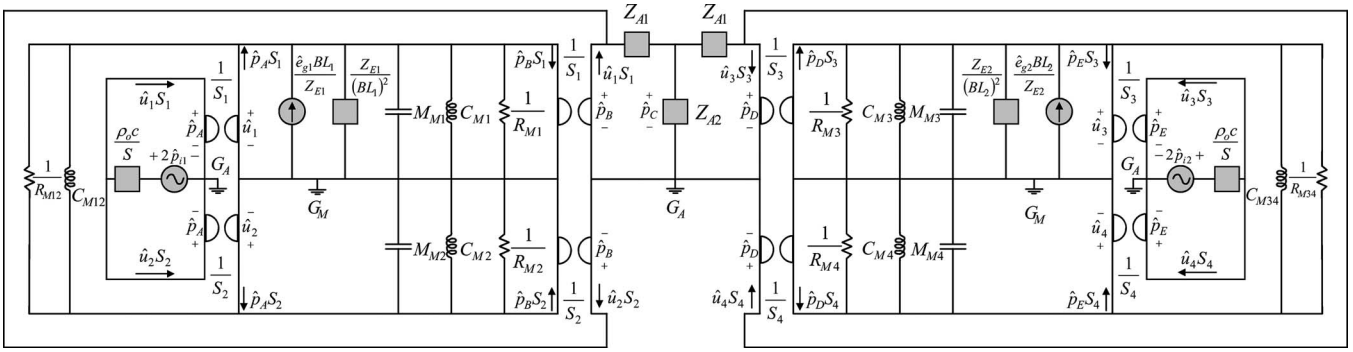

FIG. 4. Multiple-domain analogous circuit representing the ASP module.

is limited to one-dimensional modeling, as it assumes normal plane-wave incidence and transmission with respect to each panel. It also assumes steady-state time-harmonic excitation and control. However, as has been shown elsewhere, the TL predictions that result from such a circuit are well suited for comparison with classical normal-incidence TL formulations and related experimental measurements.[5,16–19]

IV. EQUATION DEVELOPMENT

Nodal analysis was used to write nine equations in nine unknowns ($\hat{u}_1$, $\hat{u}_2$, $\hat{u}_3$, $\hat{u}_4$, $\hat{p}_A$, $\hat{p}_B$, $\hat{p}_C$, $\hat{p}_D$, and $\hat{p}_E$) for the circuit:

$$\frac{\hat{e}_{g1}BL_1}{Z_{E1}} + (\hat{p}_A - \hat{p}_B)S_1 - (\hat{u}_1 - \hat{u}_2)Z_{M12} - \hat{u}_1 Z_{M1} = 0, \tag{2}$$

$$(\hat{p}_A - \hat{p}_B)S_2 + (\hat{u}_1 - \hat{u}_2)Z_{M12} - \hat{u}_2 Z_{M2} = 0, \tag{3}$$

$$\hat{p}_A = 2\hat{p}_{i1} - \hat{U}_1 \frac{\rho_0 c}{S}, \tag{4}$$

$$\hat{U}_1 - \frac{(\hat{p}_B - \hat{p}_C)}{Z_{A1}} = 0, \tag{5}$$

$$\frac{(\hat{p}_B - \hat{p}_C)}{Z_{A1}} - \frac{(\hat{p}_C - \hat{p}_D)}{Z_{A1}} - \frac{\hat{p}_C}{Z_{A2}} = 0, \tag{6}$$

$$\frac{(\hat{p}_C - \hat{p}_D)}{Z_{A1}} - \hat{U}_2 = 0, \tag{7}$$

$$\frac{\hat{e}_{g2}BL_2}{Z_{E2}} + (\hat{p}_D - \hat{p}_E)S_3 - (\hat{u}_3 - \hat{u}_4)Z_{M34} - \hat{u}_3 Z_{M3} = 0, \tag{8}$$

$$(\hat{p}_D - \hat{p}_E)S_4 + (\hat{u}_3 - \hat{u}_4)Z_{M34} - \hat{u}_4 Z_{M4} = 0, \tag{9}$$

$$\hat{p}_E = 2\hat{p}_{i2} - \hat{U}_2 \frac{\rho_0 c}{S}. \tag{10}$$

Six mechanical impedance substitutions (Z_{M1}, Z_{M2}, Z_{M3}, Z_{M4}, Z_{M12}, and Z_{M34}) are used in the above equations and are defined in the Appendix. The nine nodal equations can be reduced to four coupled equations of motion with $\hat{u}_1$, $\hat{u}_2$, $\hat{u}_3$, and $\hat{u}_4$ as the unknown variables. The solution to the equations of motion for these variables required careful algebraic reduction by means of impedance substitutions. The full solution is much too lengthy to include in this paper. Instead, the primary governing equations are presented in the body of the paper and all of the algebraic impedance substitutions are defined in the Appendix. The impedance definitions were created and labeled sequentially (with subscripts) during the solution process with the following letter order: *B*, *C*, *D*, and *F* (the letters *A* and *E* were skipped to avoid confusion with acoustic and electrical impedance definitions). The reader should be aware that the impedance substitutions are not intended to have specific physical significance, but are primarily used to enable the presentation of a compact solution.

Several quantities of interest can be obtained from the model. It will first be used to predict both plant FRFs. The plant FRFs can be used to design a new controller or to evaluate the stability margins of an existing controller. Second, the model is used to estimate the acoustic coupling strength between the two panels. This is accomplished by looking at the FRF between the control voltage of one actuator and the acceleration of the other panel. (It is expected that an acoustic coupling path will exist between the panels, but that its effect will not require coupled feedback controllers.) Third, the model is used to predict the unidirectional TL through the module. This is accomplished by letting $\hat{p}_{i1}$ equal 1 Pa while $\hat{p}_{i2}$ is set to zero for the left-to-right TL and vice versa for the right-to-left TL. Finally, the model is used to predict the bidirectional capabilities of the module. This is accomplished by letting both $\hat{p}_{i1}$ and $\hat{p}_{i2}$ be arbitrarily defined over different frequency bands.

A. Plant FRFs

Knowledge of the plant FRF *P* allows for the design of an appropriate controller. Two plants exist in this model (one for each panel) and are defined here as the frequency response from the input control voltage of an actuator to the output of the error-sensing accelerometer:

$$P(f) = \frac{\text{accelerometer output}}{\text{actuator input}}. \tag{11}$$

The voltage output of the panel-mounted accelerometer was used as the error signal for the feedback controller. The solution of the equations of motion yields the normal surface velocity for each panel:

$$\hat{u}_1 = 2\hat{p}_{i1}Z_{D1} + 2\hat{p}_{i2}Z_{D7} + \hat{e}_{g1}BL_1 Z_{D2} + \hat{e}_{g2}BL_2 Z_{D3}, \tag{12}$$

$$\hat{u}_3 = 2\hat{p}_{i1}Z_{F1} + 2\hat{p}_{i2}(Z_{F4} - Z_{F5}) + \hat{e}_{g1}BL_1 Z_{F3} + \hat{e}_{g2}BL_2 Z_{F2}. \tag{13}$$

The acceleration of each panel can then be found by using the simple relationships

$$\hat{a}_1 = j\omega\hat{u}_1, \tag{14}$$

$$\hat{a}_3 = j\omega\hat{u}_3. \tag{15}$$

The accelerance FRF of the first plant (between $\hat{e}_{g1}$ and $\hat{a}_1$) is readily found from Eqs. (12) and (14) by setting $\hat{p}_{i1}$, $\hat{p}_{i2}$, and $\hat{e}_{g2}$ equal to zero:

$$P_{11} = \frac{\hat{a}_1}{\hat{e}_{g1}} = j\omega BL_1 Z_{D2}. \tag{16}$$

Similarly, the accelerance FRF of the second plant (between $\hat{e}_{g2}$ and $\hat{a}_3$) can be found from Eqs. (13) and (15) by setting $\hat{p}_{i1}$, $\hat{p}_{i2}$, and $\hat{e}_{g1}$ equal to zero:

$$P_{22} = \frac{\hat{a}_3}{\hat{e}_{g2}} = j\omega BL_2 Z_{F2}. \tag{17}$$

The output voltages of the ideal accelerometers are considered to be equivalent to $\hat{a}_1$ and $\hat{a}_3$.

B. Acoustic coupling FRFs

The two halves of the module in this analysis are assumed to be structurally isolated from one another so that the only physical coupling path between them is through the air cavity. The magnitude of the acoustic coupling FRF will be large when resonances exist. A qualitative measure of the strength of this coupling path is the FRF between the acceleration of one panel due to an excitation of the other panel. It can be found by using Eqs. (12)–(15) and by solving for the cross FRFs, meaning the acceleration of one panel due to a control voltage on the other actuator (after $\hat{p}_{i1}$, $\hat{p}_{i2}$, and the uninvolved control voltage is set to zero):

$$P_{21} = \frac{\hat{a}_1}{\hat{e}_{g2}} = j\omega BL_2 Z_{D3}, \tag{18}$$

$$P_{12} = \frac{\hat{a}_3}{\hat{e}_{g1}} = j\omega BL_1 Z_{F3}. \tag{19}$$

C. TL

The TL of the module is defined in terms of the time-averaged incident sound power, $\langle \Pi_i \rangle_t$, and the time-averaged transmitted sound power $\langle \Pi_t \rangle_t$:[43]

$$\mathrm{TL} = 10 \log\left(\frac{\langle \Pi_i \rangle_t}{\langle \Pi_t \rangle_t}\right). \tag{20}$$

Since the total surface area of side 1 is the same as the total surface area of side 2 (i.e., $S=S_1+S_2=S_3+S_4$) and since plane-wave propagation is assumed, Eq. (20) can be reduced to

$$\mathrm{TL} = 10 \log\left(\left|\frac{\hat{p}_{in}}{\hat{p}_{tm}}\right|^2\right), \tag{21}$$

where $\hat{p}_{in}$ is the incident pressure on side n and $\hat{p}_{tm}$ is the transmitted pressure on side m due to $\hat{p}_{in}$. For the left-to-right TL through the module, $\hat{p}_{in}$ is $\hat{p}_{i1}$ and $\hat{p}_{tm}$ is $\hat{p}_{t2}$. For the normal one-dimensional field, the pressure $\hat{p}_{t2}$ is equal to the product of the total volume velocity of side 2, $\hat{U}_2$, and the acoustic impedance $\rho_0 c/S$ seen by the module on side 2 (assumed to be anechoic). Manipulation of the analogous circuit equations presented at the beginning of Sec. IV yields the left-to-right TL through the module:

$$\mathrm{TL}_{12} = 10 \log_{10}\left(\left|\frac{\hat{p}_{i1}S}{(\rho_0 c)\left[2\hat{p}_{i1}(Z_{A2}Z_{B1})(S_1Z_{D1}-S_2Z_{D4}) + 2\hat{p}_{i2}[Z_{A2}Z_{B1}(S_1Z_{D7}-S_2Z_{D8})-Z_{B1}] + \hat{e}_{g1}BL_1(Z_{A2}Z_{B1})(S_1Z_{D2}-S_2Z_{D5}) + \hat{e}_{g2}BL_2\left[Z_{A2}Z_{B1}(S_1Z_{D3}-S_2Z_{D6}) + \frac{Z_{B2}}{Z_{E2}}\right]\right]}\right|^2\right). \tag{22}$$

If $\hat{p}_{i2}$ were zero, the equation would reduce to the unidirectional left-to-right (side 1 to side 2) TL through the module based solely on the disturbance pressure $\hat{p}_{i1}$. The presence of $\hat{p}_{i2}$ acts to reduce the "measurable," though perhaps not "perceived," TL through the module because an observer on side 2 may not distinguish the time-harmonic sound pressure transmitted through the module due to $\hat{p}_{i1}$ from the time-harmonic sound pressure at the same frequency reflected from panel 2 due to $\hat{p}_{i2}$. Equation (22) can also predict the TL of the module in its passive configuration (with both $\hat{e}_{g1}$ and $\hat{e}_{g2}$ set equal to zero and both Z_{E1} and Z_{E2} set to infinity to represent open-circuit actuator terminals). It can further predict the TL of a configuration with only a single-panel active (either $\hat{e}_{g1}$ or $\hat{e}_{g2}$ equal to zero and either Z_{E1} and Z_{E2} set to infinity, respectively) or a configuration with both panels active (both $\hat{e}_{g1}$ and $\hat{e}_{g2}$ nonzero and $Z_{En}=R_g+R_{En}+j\omega L_{En}$). Alternatively, the right-to-left TL through the module is given, using the defined impedance substitutions, by the expression

$$\mathrm{TL}_{21} = 10 \log_{10}\left(\left|\frac{\hat{p}_{i2}S}{(\rho_0 c)[2\hat{p}_{i1}(S_1Z_{D1}-S_2Z_{D4}) + 2\hat{p}_{i2}(S_1Z_{D7}-S_2Z_{D8}) + \hat{e}_{g1}BL_1(S_1Z_{D2}-S_2Z_{D5}) + \hat{e}_{g2}BL_2(S_1Z_{D3}-S_2Z_{D6})]}\right|^2\right). \tag{23}$$

The control voltages in Eqs. (22) and (23) are given by the products of the panel accelerations and the FRFs of the control circuits:

$$\hat{e}_{g1} = j\omega H_1 \hat{u}_1, \tag{24}$$

$$\hat{e}_{g2} = j\omega H_2 \hat{u}_3. \tag{25}$$

One can substitute Eqs. (12) and (13) for $\hat{u}_1$ and $\hat{u}_2$ in these expressions, then the resulting expressions can be solved simultaneously for the control voltages $\hat{e}_{g1}$ and $\hat{e}_{g2}$ in terms of

the incident pressures. The appropriate terms need to be set equal to zero or infinity for the specific control configuration. For example, if only panel 1 is actively controlled and there is only a single disturbance source $\hat{p}_{i1}$, then $\hat{p}_{i2}$ and $\hat{e}_{g2}$ in Eq. (12) would be set to zero and Z_{E2} would be set to infinity. Equations (12) and (24) would then yield the following control voltage:

$$\hat{e}_{g1} = \frac{2\hat{p}_{i1} j\omega H_1 Z_{D1}}{1 - j\omega H_1 B L_1 Z_{D2}}. \tag{26}$$

Control voltages for the other configurations can be determined in a similar fashion. In each case, $\hat{e}_{g1}$ and $\hat{e}_{g2}$ represent the actual electrical voltages that drive the actuators. They do not necessarily represent control voltages that will completely force $\hat{u}_1$ and $\hat{u}_3$ to be zero.

D. Bidirectional TL

The equations presented in Sec. IV C can also predict the "bidirectional" TL through the module. In this context, the term bidirectional refers to the situation in which disturbance pressures are simultaneously incident on each side of the module. One must therefore speak in terms of the "measurable" TL because the ability to observe and separate the incident, reflected, and transmitted pressures depends on the nature of the disturbances. For example, the TL can be observed as usual when $\hat{p}_{i1}$ and $\hat{p}_{i2}$ contain different frequencies or when they contain the same frequencies but at dramatically different amplitudes. However, the second disturbance source will reduce the measurable TL through the module when both $\hat{p}_{i1}$ and $\hat{p}_{i2}$ possess the same frequencies with similar amplitudes. This is because one cannot readily separate the pressure that is transmitted through the module (from disturbance source 1) from the reflected pressure (from disturbance source 2).

V. MODEL PREDICTIONS

The predictive capabilities of the model may be illustrated using representative numerical module parameters. Table I lists several feasible values for the enhanced loudspeaker model, with the assumption that both halves of the module use identical components ($BL_1 = BL_2$, $L_{E1} = L_{E2}$, etc.). It also lists a frequency-dependent attenuation coefficient α, given in Np/m, for hypothetical damping within the cavity. The damping is then included in the model through the complex wave number. The module cavity depth L is chosen to be 15 cm and its total cross-sectional area S is chosen to be 33 cm^2.

TABLE I. Enhanced model parameters and frequency-dependent attenuation coefficient used in the numerical analysis.

Parameter	Value	Units
BL_1, BL_2	3.54	Tm
L_{E1}, L_{E2}	0.23	mH
R_{E1}, R_{E2}	6.48	Ω
R_{g1}, R_{g2}	0.10	Ω
S_1, S_3	30.0	cm^2
S_2, S_4	3.00	cm^2
M_{M1}, M_{M3}	7.21	g
M_{M2}, M_{M4}	0.15	g
C_{M1}, C_{M3}	2300	μm/N
C_{M2}, C_{M4}	448	μm/N
C_{M12}, C_{M34}	272	μm/N
R_{M1}, R_{M3}	0.57	kg/s
R_{M2}, R_{M4}	0.30	kg/s
R_{M12}, R_{M34}	0.30	kg/s

Frequency band	α (Np/m)
$f \leq 500$ Hz	0.1
$500 < f \leq 1000$ Hz	0.4
$1000 < f \leq 1300$ Hz	0.9
$f > 1300$ Hz	1.0

A. Predicted plant FRFs

The normalized accelerance FRF P_{11} predicted by Eq. (16) is shown in Fig. 5. This curve represents the acceleration seen by panel 1 due to an actuator excitation voltage $\hat{e}_{g1}$. Since panel 2 has the same parameters as panel 1, P_{22} is identical to P_{11}. The first peak seen near 80 Hz is the primary mechanical resonance of the panel with its attached moving-coil actuator. The magnitude of the FRF falls off at 12 dB per octave below this frequency. The second peak near 185 Hz is the mass-air-mass resonance frequency of the double-panel partition. The magnitude of the FRF is relatively flat above the mass-air-mass resonance frequency until it begins to roll off at high frequencies due to the inductance of the actuator voice coil.

The accelerance FRF can be used to design a controller or to test the stability margins of an existing controller. For the control circuit described earlier, the resistor and capacitor values were chosen to position the cutoff frequencies of the control filter and thus maximize attenuation while maintaining desired stability margins.[20–22] The selected values are given in Table II, and the frequency response of the resulting controller is shown in Fig. 6. The controller is primarily a low-pass filter, with an asymptotic attenuation approaching 20 dB above 20 kHz. A notch was also designed into the controller that can be strategically placed at a desired panel resonance (through selected resistor and capacitor values) to

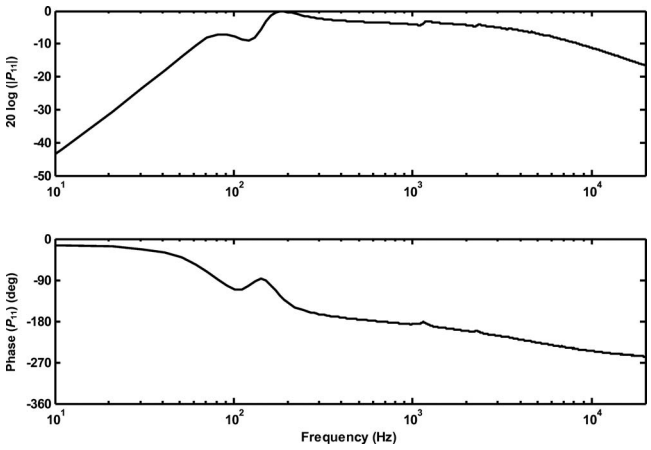

FIG. 5. Normalized accelerance FRF for the module.

TABLE II. Resistor and capacitor values used in the analog controller.

Parameter	Value	Units
R_0	10 000	Ω
R_1	430	Ω
R_2	13 120	Ω
R_3	1 000	Ω
R_4	452	Ω
R_5	10 000	Ω
R_6	1 300	Ω
C_1	0.047	μF
C_2	0.047	μF

allow the closed-loop response of the system to become smoother. Figure 6 shows the notch centered at 3 kHz.

B. Predicted acoustic coupling FRFs

The cross-coupling FRF P_{12} between the acceleration of one panel due to the input excitation of the other is shown in Fig. 7. The mass-air-mass resonance is evident at 185 Hz and represents the strongest coupling from one panel to the other. The axial cavity resonances are also clearly evident with the first resonance occurring near 1.1 kHz. However, the magnitude of the first cavity resonance is nearly 20 dB down from the mass-air-mass resonance. The P_{21} cross-coupling FRF is identical to the one shown in Fig. 7.

The effect of the cavity depth L on the acoustic coupling strength was investigated to explore its impact. The results for three different cavity depths are shown in Fig. 8. The peak magnitude of the acoustic coupling FRF increased by roughly 3 dB per halving of distance. The magnitude was independent of L at frequencies well below the mass-air-mass resonance. The general trend of P_{12} was also independent of L at frequencies far above the first axial cavity resonance (excluding, of course, the frequency-dependent location of the peaks that varied with L). The cross-coupling FRFs indicate that the acoustic coupling between the panels is weak at all frequencies other than the mass-air-mass resonance frequency.

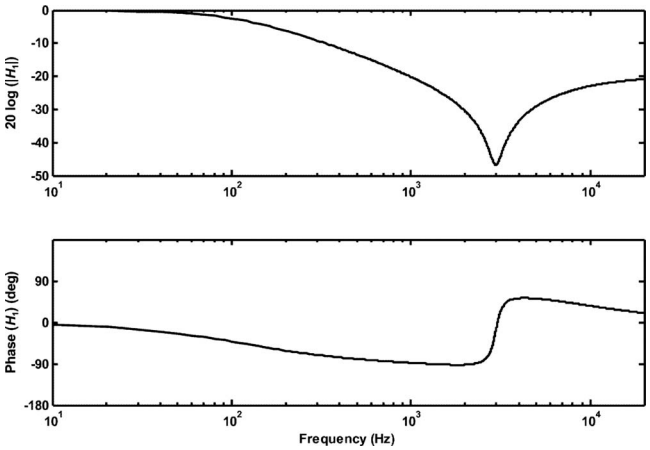

FIG. 6. Predicted FRF of the controller.

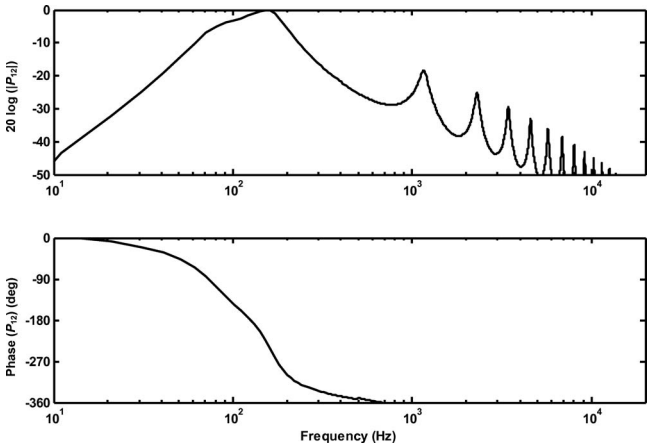

FIG. 7. Cross-coupling accelerance FRF.

C. Predicted TL

The unidirectional TL (e.g., from left-to-right) through the module is plotted in Fig. 9 for three control configurations. The passive configuration exhibits the characteristic response of a double-panel partition.[1] The TL increases at 18 dB per octave immediately above the mass-air-mass resonance frequency while the slope decreases slightly to 12 dB per octave at higher frequencies. The axial cavity resonances are also clearly seen.

The prediction for single-panel control is also shown in the figure and is the same regardless of whether panel 1 or panel 2 is actively controlled while the other panel remains passive. The controllers were designed such that the module transitions to a completely passive state at frequencies higher than about 1 kHz. The maximum increase in TL for this configuration is 27 dB at 165 Hz. The arithmetic average increase from 50 to 500 Hz is 18 dB. This represents a considerable improvement in low-frequency TL, even with only a single controlled panel. The control does not completely eliminate the TL effect caused by the strong acoustic coupling between panels at the mass-air-mass resonance frequency. Any uncontrolled residual vibration that exists on the first panel is readily transmitted to the second panel in the vicinity of the resonance.

The predicted TL increases further in the third control configuration when both panels are controlled independently

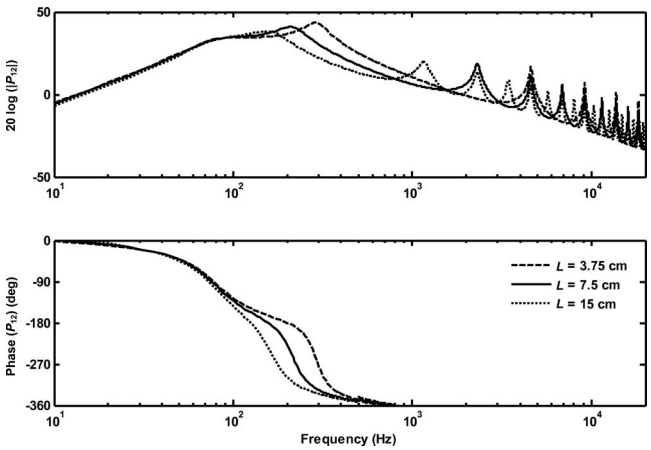

FIG. 8. Cross-coupling accelerance FRFs for three different cavity depths.

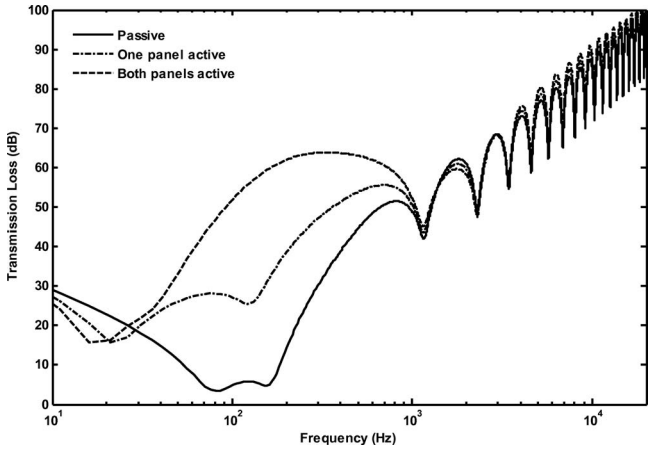

FIG. 9. Predicted unidirectional TL through the module.

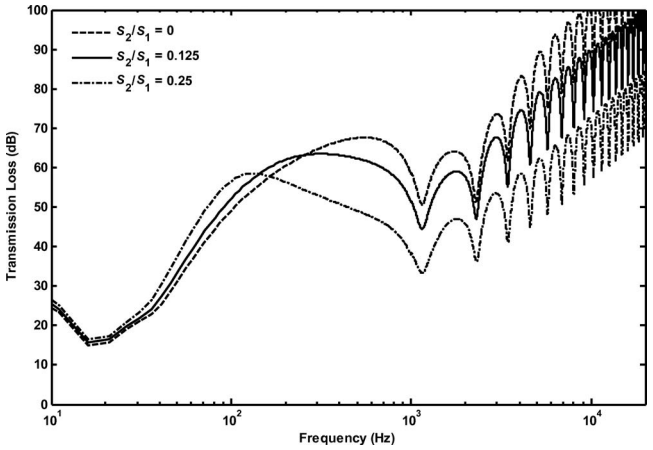

FIG. 10. Effect of the area ratio S_2/S_1 on TL when both panels are actively controlled.

but simultaneously. The maximum increase is 55 dB at 165 Hz. The average increase in the TL from 50 to 500 Hz is 36 dB—twice that produced by the single-panel control. The effect of the mass-air-mass resonance is no longer apparent.

The TL for both active cases was slightly lower than the passive case between 10 and 25 Hz. The dips in the TL curves in this region are an effect of the feedback controller, as these frequencies are near the lower instability point of the closed-loop feedback control system. At these frequencies, the control signal is nearly in phase with the disturbance signal, resulting in a slight degradation in the TL.

One should recall that the enhanced loudspeaker model permits the surround to respond with an additional DOF not represented in the classical model. It is conceivable that a surround could thus vibrate freely at some frequency even when its associated panel is not vibrating. The effect of the ratio of surround area to panel area on TL was explored with this effect in mind. Three different ratios of S_2/S_1 (and likewise S_4/S_3) were examined for the case when both panels were actively controlled. The total cross-sectional area of the module S was kept at 33 cm^2 and the ratio of S_2/S_1 was varied to produce ratios of 0, 0.125, and 0.250. The results are shown in Fig. 10. The degradation of the TL when S_2 is increased is substantial above 150 Hz. The TL prediction from the classical model of the loudspeaker is the same as the $S_2/S_1=0$ curve (i.e., no surround area). To obtain the best overall TL, the areas that are not directly actuated (S_2 and S_4) should be minimized while maintaining sufficient resilience for isolation of interstitial structures and adjacent panels.

The effect of cavity depth on TL was also explored. It was shown earlier that the acoustic coupling strength increases in the vicinity of the mass-air-mass resonance as the space between the panels is diminished. This reduces the TL that can be achieved in the control bandwidth. The predicted TL for three different cavity depths is shown in Fig. 11. It was found that the average achievable TL in the control bandwidth (20 Hz–1 kHz) increases by approximately 6 dB each time the cavity depth (L) is doubled. The low- and high-frequency regions of the TL curve remain essentially unaffected by the depth (although the cavity resonances shift in frequency).

The right-to-left unidirectional TLs for the module are exactly the same as the results presented above. This represents a significant advancement over other active methods. The physical configuration and independent controllers enable the module to exhibit the same unidirectional TL in both directions.

D. Predicted bidirectional TL

The final performance test of the ASP module explores how the TL is affected when pressure disturbances $\hat{p}_{i1}$ and $\hat{p}_{i2}$ exist simultaneously on both sides. (Section V C showed the results for the unidirectional TL that results when only $\hat{p}_{i1}$ or $\hat{p}_{i2}$ was present.) Suppose the primary disturbance source is $\hat{p}_{i1}$ and impinges on the left side of the module. The TL from left-to-right through the module is given in Eq. (22). If the pressure $\hat{p}_{i2}$ on the right side of the module is zero, then the equation reduces to the left-to-right unidirectional TL. The measurable left-to-right TL of the module becomes degraded if $\hat{p}_{i2}$ is nonzero. The degradation only occurs at frequencies contained in $\hat{p}_{i2}$, and the amount of degradation depends on the amplitude of $\hat{p}_{i2}$ relative to $\hat{p}_{i1}$.

For the sake of illustration, suppose $\hat{p}_{i1}$ has a real value of 1 Pa at all frequencies and $\hat{p}_{i2}$ is zero everywhere outside the arbitrary bandwidth of 200–400 Hz, but is allowed to take on various real values within that bandwidth: 0, 0.1, 1.0, and 10 Pa. The apparent TL with both panels actively con-

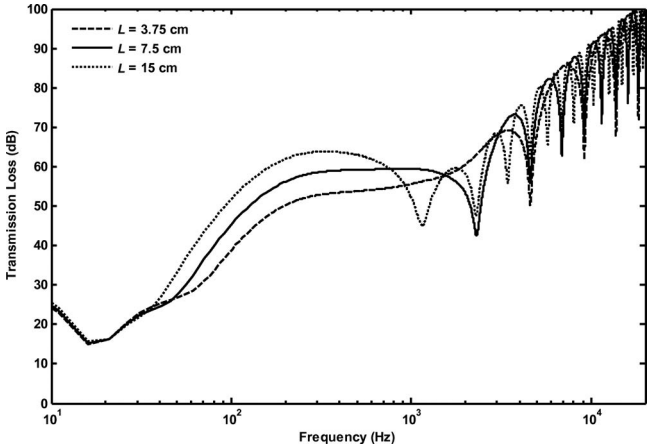

FIG. 11. Effect of cavity depth L on TL when both panels are actively controlled.

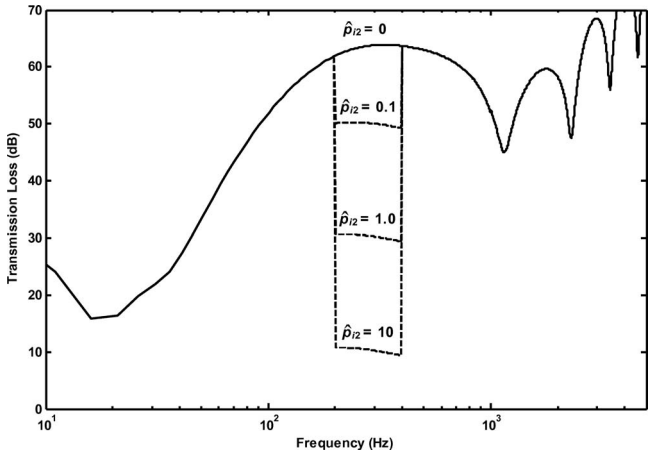

FIG. 12. Apparent left-to-right TL through the module when a second disturbance source of different amplitude is present.

trolled is shown in Fig. 12. It is apparent from this example that the measurable TL is reduced when a second disturbance source is present on the receiving side of the module, but the reduction depends on the relative amplitude of the source. It is not affected outside of the bandwidth of $\hat{p}_{i2}$. The controlled module is actually attenuating the sound energy passing through it from left to right, but the presence of a second source on the receiving side inhibits the ability to quantify the TL. In many cases, acoustic observation in a common excitation bandwidth and on a given side of the module could be dominated by the acoustic source that resides on that side.

VI. CONCLUSION

The performance of a feedback-controlled double-panel ASP module was examined using analytical tools and numerical calculations. An enhanced model of a loudspeaker was used to model each half of the ASP module, wherein the surround possessed an additional DOF. Equations were developed to estimate the plant FRFs, understand the effects of acoustic coupling between the panels, predict the TL of the module in both passive and active states, and demonstrate that the module design produces bidirectional TL.

It was shown that the TL for the passive double-panel module exhibited the classical resonance effects at low frequencies. Active feedback control of a single panel produced an average TL boost of 18 dB from 50 to 500 Hz. However, the mass-air-mass resonance dip was still apparent in the predicted TL curve due to the strong acoustic coupling in the cavity near its center frequency. Simultaneous active feedback control of both panels produced an average boost in the TL of 36 dB from 50 to 500 Hz. It also eliminated the TL dip at the mass-air-mass resonance frequency.

The enhanced model of the loudspeaker illustrates the effect of having an uncontrolled vibrating surface area as part of the panel. The surround of the panel is still permitted to vibrate even if the vibration of the panel is reduced. The residual vibration of the surround permits flanking around the panel and degrades its TL performance. This effect can be reduced by minimizing the area of the surround.

The cavity depth also affects the maximum achievable TL. Smaller cavity depths intensify the acoustic coupling between the panels. On average, the achievable TL in the control bandwidth is reduced by 6 dB every time the cavity depth is cut in half. The TL at frequencies well below the mass-air-mass resonance is not affected, nor is the general TL trend affected at sufficiently high frequencies above the control bandwidth.

The ASP module design and analysis presented in this paper demonstrate that simultaneous feedback control of each panel in a double-panel configuration provides an effective way to actively increase TL at low frequencies. The design transitions to passive TL control at higher frequencies, which is inherently effective for sound isolation. It also enables bidirectional TL capabilities over all frequencies. For future research, an experimental embodiment of the module should be constructed and tested. An array of such modules should also be constructed and tested as a complete partition between adjacent three-dimensional spaces.

ACKNOWLEDGMENTS

The authors gratefully acknowledge financial support from the Department of Mechanical Engineering at Brigham Young University as well as the NASA Rocky Mountain Space Grant Consortium.

Nomenclature

$\hat{a}_n$ = normal complex acceleration amplitude of the nth panel
BL_n = force factor of the nth moving-coil actuator
c = speed of sound in the fluid medium
c_{ph} = phase speed of sound in a dissipative medium
C_n = electrical capacitance of the nth capacitor in the control circuit
C_{Mn} = effective mechanical compliance of the nth module element
C_{Mmn} = effective mechanical compliance coupling the mth and nth module elements ($m=n$)
$\hat{e}_{gn}$ = complex control voltage amplitude driving the nth moving-coil driver
f = frequency
G_A = acoustical ground (ambient reference pressure)
G_M = mechanical ground (zero reference velocity)
H_n = complex FRF of the nth controller
$\tilde{k}$ = complex acoustic wave number, $=\omega/c_{\mathrm{ph}} - j\alpha$
L = effective cavity length of the module
L_{En} = electrical inductance of the voice coil in the nth moving-coil actuator
m = integer index value
M_{Mn} = effective mechanical mass of the nth module element
n = integer index value
$\hat{p}_q$ = complex acoustic pressure amplitude at location q in the analogous circuit

$\hat{p}_{in}$ = normally incident complex acoustic pressure amplitude on the nth side of the module

$\hat{p}_{tm}$ = normal transmitted complex acoustic pressure amplitude on the mth side of the module

P_{mn} = plant or coupling FRF from the side m actuator input to the side n error sensor output

R_n = electrical resistance of the nth resistor in the control circuit

R_{En} = electrical resistance of the voice coil in the nth moving-coil actuator

R_g = output resistance of the electrical control source

R_{Mn} = effective mechanical resistance of the nth module element

R_{Mmn} = effective mechanical resistance coupling the mth and nth module elements $(m \neq n)$

S = total cross-sectional area of the module, $=S_1+S_2=S_3+S_4$

s = Laplace domain frequency variable

S_n = cross-sectional area of the nth module element

TL = normal-incidence sound transmission loss

$\hat{u}_n$ = complex normal velocity amplitude of the nth module element

$\hat{U}_n$ = complex volume velocity amplitude on the nth side of module, e.g., $\hat{U}_1=\hat{u}_1S_1+\hat{u}_2S_2$

Z_{A1} = acoustic impedance substitution for waveguide network, $=j(\omega\rho_o/\tilde{k}S)\tan(\tilde{k}L/2)$

Z_{A2} = acoustic impedance substitution for waveguide network, $=-j(\omega\rho_o/\tilde{k}S)\csc(\tilde{k}L)$

Z_{En} = total electrical impedance of the nth moving-coil actuator, $=R_g+R_{En}+j\omega L_{En}$

α = attenuation coefficient of the absorptive material used in the cavity (Np/m)

ρ_0 = ambient density of the fluid medium

ω = angular frequency$=2\pi f$

Π = acoustic sound power

APPENDIX: IMPEDANCE DEFINITIONS

Mechanical impedance substitutions:

$$Z_{M1} \equiv \frac{(BL_1)^2}{Z_{E1}} + R_{M1} + \frac{1}{j\omega C_{M1}} + j\omega M_{M1}, \tag{A1}$$

$$Z_{M2} \equiv R_{M2} + \frac{1}{j\omega C_{M2}} + j\omega M_{M2}, \tag{A2}$$

$$Z_{M3} \equiv \frac{(BL_2)^2}{Z_{E2}} + R_{M3} + \frac{1}{j\omega C_{M3}} + j\omega M_{M3}, \tag{A3}$$

$$Z_{M4} \equiv R_{M4} + \frac{1}{j\omega C_{M4}} + j\omega M_{M4}, \tag{A4}$$

$$Z_{M12} \equiv R_{M12} + \frac{1}{j\omega C_{M12}}, \tag{A5}$$

$$Z_{M34} \equiv R_{M34} + \frac{1}{j\omega C_{M34}}, \tag{A6}$$

$$Z_{M1.PR} \equiv Z_{M1} + Z_{M12}, \tag{A7}$$

$$Z_{M2.PR} \equiv Z_{M2} + Z_{M12}, \tag{A8}$$

$$Z_{M3.PR} \equiv Z_{M3} + Z_{M34}, \tag{A9}$$

$$Z_{M4.PR} \equiv Z_{M4} + Z_{M34}. \tag{A10}$$

Acoustic impedance substitutions:

$$Z_{AA} \equiv \frac{\rho_0 c}{S} + Z_{A1} + Z_{A2}, \tag{A11}$$

$$Z_{AB} \equiv Z_{AA}. \tag{A12}$$

B impedance substitutions:

$$Z_{B1} \equiv \frac{S_3^{\,2}Z_{M4.PR} + 2S_3S_4Z_{M34} + S_4^{\,2}Z_{M3.PR}}{S_3^{\,2}Z_{AB}Z_{M4.PR} + S_4^{\,2}Z_{AB}Z_{M3.PR} + Z_{M3.PR}Z_{M4.PR} + 2S_3S_4Z_{AB}Z_{M34} - Z_{M34}^{\,2}}, \tag{A13}$$

$$Z_{B2} \equiv \frac{S_3Z_{M4.PR} + S_4Z_{M34}}{S_3^{\,2}Z_{AB}Z_{M4.PR} + S_4^{\,2}Z_{AB}Z_{M3.PR} + Z_{M3.PR}Z_{M4.PR} + 2S_3S_4Z_{AB}Z_{M34} - Z_{M34}^{\,2}}. \tag{A14}$$

C impedance substitutions:

$$Z_{C1} \equiv S_1^{\,2}Z_{A2}^{\,2}Z_{B1} - S_1^{\,2}Z_{AA} - Z_{M1.PR}, \tag{A15}$$

$$Z_{C2} \equiv S_1S_2Z_{A2}^{\,2}Z_{B1} + Z_{M12} - S_1S_2Z_{AA}, \tag{A16}$$

$$Z_{C3} \equiv S_2^{\,2}Z_{A2}^{\,2}Z_{B1} - S_2^{\,2}Z_{AA} - Z_{M2.PR}. \tag{A17}$$

D impedance substitutions:

$$Z_{D1} \equiv \frac{Z_{E1}Z_{E2}(S_1Z_{C3} - S_2Z_{C2})}{Z_{E1}Z_{E2}(Z_{C2}^{\,2} - Z_{C1}Z_{C3})}, \tag{A18}$$

$$Z_{D2} \equiv \frac{Z_{E2}(Z_{C3})}{Z_{E1}Z_{E2}(Z_{C2}{}^2 - Z_{C1}Z_{C3})}, \tag{A19}$$

$$Z_{D3} \equiv \frac{Z_{E1}Z_{A2}Z_{B2}(S_1Z_{C3} - S_2Z_{C2})}{Z_{E1}Z_{E2}(Z_{C2}{}^2 - Z_{C1}Z_{C3})}, \tag{A20}$$

$$Z_{D4} \equiv \frac{Z_{E1}Z_{E2}(S_1Z_{C2} - S_2Z_{C1})}{Z_{E1}Z_{E2}(Z_{C2}{}^2 - Z_{C1}Z_{C3})}, \tag{A21}$$

$$Z_{D5} \equiv \frac{Z_{E2}(Z_{C2})}{Z_{E1}Z_{E2}(Z_{C2}{}^2 - Z_{C1}Z_{C3})}, \tag{A22}$$

$$Z_{D6} \equiv \frac{Z_{E1}Z_{A2}Z_{B2}(S_1Z_{C2} - S_2Z_{C1})}{Z_{E1}Z_{E2}(Z_{C2}{}^2 - Z_{C1}Z_{C3})}, \tag{A23}$$

$$Z_{D7} \equiv \frac{Z_{E1}Z_{E2}Z_{A2}Z_{B1}(S_2Z_{C2} - S_1Z_{C3})}{Z_{E1}Z_{E2}(Z_{C2}{}^2 - Z_{C1}Z_{C3})}, \tag{A24}$$

$$Z_{D8} \equiv \frac{Z_{E1}Z_{E2}Z_{A2}Z_{B1}(S_2Z_{C1} - S_1Z_{C2})}{Z_{E1}Z_{E2}(Z_{C2}{}^2 - Z_{C1}Z_{C3})}. \tag{A25}$$

F impedance substitutions:

$$Z_{F1} \equiv \frac{(S_1Z_{D1} - S_2Z_{D4})(S_3Z_{A2}Z_{E2}Z_{M4.PR} + S_4Z_{M34}Z_{A2}Z_{E2})}{Z_{E2}(S_3{}^2Z_{AB}Z_{M4.PR} + S_4{}^2Z_{AB}Z_{M3.PR} + Z_{M3.PR}Z_{M4.PR} + 2S_3S_4Z_{AB}Z_{M34} - Z_{M34}{}^2)}, \tag{A26}$$

$$Z_{F2} \equiv \frac{(S_1Z_{D3} - S_2Z_{D6})(S_3Z_{A2}Z_{E2}Z_{M4.PR} + S_4Z_{M34}Z_{A2}Z_{E2}) + (S_4{}^2Z_{AB} + Z_{M4.PR})}{Z_{E2}(S_3{}^2Z_{AB}Z_{M4.PR} + S_4{}^2Z_{AB}Z_{M3.PR} + Z_{M3.PR}Z_{M4.PR} + 2S_3S_4Z_{AB}Z_{M34} - Z_{M34}{}^2)}, \tag{A27}$$

$$Z_{F3} \equiv \frac{(S_1Z_{D2} - S_2Z_{D5})(S_3Z_{A2}Z_{E2}Z_{M4.PR} + S_4Z_{M34}Z_{A2}Z_{E2})}{Z_{E2}(S_3{}^2Z_{AB}Z_{M4.PR} + S_4{}^2Z_{AB}Z_{M3.PR} + Z_{M3.PR}Z_{M4.PR} + 2S_3S_4Z_{AB}Z_{M34} - Z_{M34}{}^2)}, \tag{A28}$$

$$Z_{F4} \equiv \frac{(S_1Z_{D7} - S_2Z_{D8})(S_3Z_{A2}Z_{E2}Z_{M4.PR} + S_4Z_{M34}Z_{A2}Z_{E2})}{Z_{E2}(S_3{}^2Z_{AB}Z_{M4.PR} + S_4{}^2Z_{AB}Z_{M3.PR} + Z_{M3.PR}Z_{M4.PR} + 2S_3S_4Z_{AB}Z_{M34} - Z_{M34}{}^2)}, \tag{A29}$$

$$Z_{F5} \equiv \frac{Z_{E2}(S_3Z_{M4.PR} + S_4Z_{M34})}{Z_{E2}(S_3{}^2Z_{AB}Z_{M4.PR} + S_4{}^2Z_{AB}Z_{M3.PR} + Z_{M3.PR}Z_{M4.PR} + 2S_3S_4Z_{AB}Z_{M34} - Z_{M34}{}^2)}. \tag{A30}$$

[1]F. Fahy, *Sound and Structural Vibration: Radiation, Transmission, and Response* (Academic, London, 1985).
[2]L. L. Beranek and I. L. Vér, *Noise and Vibration Control Engineering: Principles and Applications* (Wiley, New York, 1992).
[3]D. A. Bies and C. H. Hansen, *Engineering Noise Control: Theory and Practice* (Unwin Hyman, London, 1988).
[4]C. R. Fuller, C. H. Hansen, and S. D. Snyder, "Active control of sound radiation from a vibrating rectangular panel by sound sources and vibration inputs: An experimental comparison," J. Sound Vib. **148**, 355–360 (1991).
[5]T. W. Leishman and J. Tichy, "A theoretical and numerical analysis of vibration-controlled modules for use in active segmented partitions," J. Acoust. Soc. Am. **118**, 1424–1438 (2005).
[6]B. Bingham, M. J. Atalla, and N. W. Hagood, "Comparison of structural-acoustic control designs on an active composite panel," J. Sound Vib. **244**, 761–778 (2001).
[7]C. R. Fuller and R. J. Silcox, "Acoustics 1991: Active structural acoustic control," J. Acoust. Soc. Am. **91**, 519 (1992).
[8]P. Gardonio, E. Bianchi, and S. J. Elliott, "Smart panel with multiple decentralized units for the control of sound transmission. Part I: Theoretical predictions," J. Sound Vib. **274**, 163–192 (2004).
[9]P. Gardonio, E. Bianchi, and S. J. Elliott, "Smart panel with multiple decentralized units for the control of sound transmission. Part II: Design of the decentralized control units," J. Sound Vib. **274**, 193–213 (2004).
[10]S. M. Hirsch, N. E. Meyer, M. A. Westervelt, P. King, F. J. Li, M. V. Petrova, and J. Q. Sun, "Experimental study of smart segmented trim panels for aircraft interior noise control," J. Sound Vib. **231**, 1023–1037 (2000).
[11]S. M. Hirsch, J. Q. Sun, and M. R. Jolly, "Analytical study of interior noise control using segmented panels," J. Sound Vib. **231**, 1007–1021 (2000).
[12]M. E. Johnson and S. J. Elliott, "Active control of sound radiation using volume velocity cancellation," J. Acoust. Soc. Am. **98**, 2174–2186 (1995).
[13]B. Petitjean, I. Legrain, F. Simon, and S. Pauzin, "Active control experiments for acoustic radiation reduction of a sandwich panel: Feedback and feedforward investigations," J. Sound Vib. **252**, 19–36 (2002).
[14]R. L. St. Pierre, Jr., G. H. Koopman, and W. Chen, "Volume velocity control of sound transmission through composite panels," J. Sound Vib. **210**, 441–460 (1998).
[15]D. R. Thomas, P. A. Nelson, S. J. Elliott, and R. J. Pinnington, "Experimental investigation into the active control of sound transmission through stiff light composite panels," Noise Control Eng. J. **41**, 273–279 (1993).
[16]T. W. Leishman, *Active Control of Sound Transmission Through Partitions Composed of Discretely Controlled Modules* (The Pennsylvania State University, University Park, PA, 2000).
[17]T. W. Leishman and J. Tichy, "A fundamental investigation of the active control of sound transmission through segmented partition elements," INCE Conference Proceedings **103**, 137–148 (1997).
[18]T. W. Leishman and J. Tichy, "An experimental investigation of two module configurations for use in active segmented partitions," J. Acoust. Soc. Am. **118**, 1439–1451 (2005).
[19]T. W. Leishman and J. Tichy, "An experimental investigation of two active segmented partition arrays," J. Acoust. Soc. Am. **118**, 3050–3063 (2005).
[20]P. E. Fleischer and J. Tow, "Design formulas for biquad active filters using three operational amplifiers," Proc. IEEE **61**, 662–663 (1973).
[21]K. L. Su, *Analog Filters* (Kluwer Academic, Norwell, MA, 2002).
[22]M. Herpy and J.-C. Berka, *Active RC Filter Design* (Elsevier, New York, 1986).
[23]P. D. Wheeler, *Voice Communications in the Cockpit Noise Environment—*

The Role of Active Noise Reduction (Southampton University, Southampton, 1986).
[24]L. L. Beranek, *Acoustics* (McGraw-Hill, New York, 1954).
[25]M. Leach, *Introduction to Electroacoustics and Audio Amplifier Design* (Kendall-Hunt, Dubuque, IA, 2003).
[26]H. F. Olson, *Elements of Acoustical Engineering* (Van Nostrand, New York, 1940).
[27]B. E. Anderson, *Derivation of Moving-Coil Loudspeaker Parameters Using Plane Wave Tube Techniques* (Brigham Young University, Provo, UT, 2003).
[28]J. R. Ashley and M. D. Swan, "Experimental determination of low-frequency loudspeaker parameters," J. Audio Eng. Soc. **17**, 525–531 (1969).
[29]J. R. Ashley and M. D. Swan, "Improved measurement of loudspeaker parameters," in Convention of the Audio Engineering Society (1971).
[30]H. Blind, A. Phillips, and E. Geddes, "Efficient loudspeaker parameter estimation—An extension," in Convention of the Audio Engineering Society, San Francisco, CA (1992).
[31]R. C. Cabot, "Automated measurements of loudspeaker small-signal parameters," in Convention of the Audio Engineering Society, 1986, Los Angeles, CA.
[32]D. Clark, "Precision measurement of loudspeaker parameters," J. Audio Eng. Soc. **45**, 129–141 (1997).
[33]E. Geddes and A. Phillips, "Efficient loudspeaker linear and nonlinear parameter estimation," in Convention of the Audio Engineering Society, New York, NY (1991).
[34]R. Gomez-Meda, "Measurement of the Thiele-Small parameters for a given loudspeaker, without using a box," in Convention of the Audio Engineering Society, New York, NY (1991).
[35]W. J. J. Hoge, "The measurement of loudspeaker driver parameters," in Convention of the Audio Engineering Society, New York, NY (1977).
[36]D. B. J. Keele, "Sensitivity of Thiele's vented loudspeaker enclosure alignments to parameter variations," J. Audio Eng. Soc. **21**, 246–255 (1973).
[37]M. H. Knudsen, J. G. Jensen, V. Julskjaer, and P. Rubak, "Determination of loudspeaker driver parameters using a system identification technique," J. Audio Eng. Soc. **37**, 700–708 (1989).
[38]J. N. Moreno, "Measurement of loudspeaker parameters using a laser velocity transducer and 2-channel FFT analysis," J. Audio Eng. Soc. **39**, 243–249 (1991).
[39]J. D. Sagers, "Analog feedback control of an active sound transmission control module," MS thesis, Brigham Young University, Provo, UT (2008).
[40]J. Y. Chung, "Cross-spectral method of measuring acoustic intensity without error caused by instrument phase mismatch," J. Acoust. Soc. Am. **64**, 1613–1616 (1978).
[41]J. Y. Chung and D. A. Blaser, "Transfer function method of measuring in-duct acoustic properties, Part I: Theory," J. Acoust. Soc. Am. **68**, 907–913 (1980).
[42]J. Y. Chung and D. A. Blaser, "Transfer function method of measuring in-duct acoustic properties, Part II: Experiment," J. Acoust. Soc. Am. **68**, 914–921 (1980).
[43]A. D. Pierce, *Acoustics: An Introduction to Its Physical Principles and Applications* (McGraw-Hill, New York, 1981).